INTERNATIONAL JOURNAL OF HYDROGEN ENERGY 47 (2022) 8993–9003

Available online at www.sciencedirect.com

ScienceDirect

journal homepage: www.elsevier.com/locate/he

3D patterned electrodes for ultra-low platinum fuel cells

*Yifei Yang, Rui Sun, Yossef A. Elabd**

Department of Chemical Engineering, Texas A&M University, College Station, TX 77843, USA

HIGHLIGHTS

- 3D patterned electrodes *via* template-assisted electrospinning/electrospraying.
- Nanofiber-nanoparticle electrodes with well-defined hexagonal patterned arrays.
- High platinum utilization at ultra-low platinum loadings.
- 80 μm hexagonal pattern size resulted in the highest fuel cell performance.

GRAPHICAL ABSTRACT

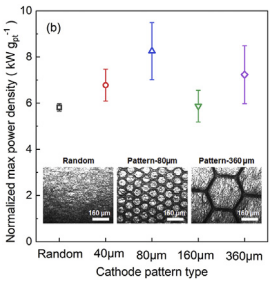

ARTICLE INFO

Article history:
Received 14 October 2021
Received in revised form
20 December 2021
Accepted 28 December 2021
Available online 17 January 2022

Keywords:
Fuel cell
Electrospinning
Electrospraying
Patterned electrodes
Nanofiber

ABSTRACT

In this study, a new fabrication technique, template-assisted electrospinning/electrospraying (E/E), was developed and successfully produced organized-structured nanofiber-nanoparticle electrodes with well-defined 3D hexagonal patterned arrays of various pattern sizes (*i.e.*, pattern diameters of 40, 80, 160, and 360 μm). At similar ultra-low platinum loadings (*ca.* 0.06 mg_{Pt} cm^{-2}), the 80 μm diameter hexagonal patterned electrodes exhibited 14% higher fuel cell power densities and 68% higher electrochemical surface area compared to the random electrode analogs (without patterns). Among different pattern sizes, electrodes with an 80 μm diameter hexagonal pattern resulted in the highest fuel cell platinum utilization and lowest electrode resistance. Additionally, patterned electrodes with smaller diameters achieved improved mechanical stiffness compared to random oriented electrodes. Compared to electrodes produced *via* conventional techniques and ink-based patterning techniques, the template-assisted E/E technique provides a versatile platform for investigating the effect of pattern type and size on fuel cell platinum utilization under ultra-low platinum loadings.

* *Corresponding author.*
E-mail address: elabd@tamu.edu (Y.A. Elabd).

https://doi.org/10.1016/j.ijhydene.2021.12.242

Introduction

Proton exchange membrane fuel cells (PEMFCs) convert chemical fuel directly into electrical energy with zero carbon dioxide emission [1–3]. Although PEMFC vehicles are now commercially available, the high amounts or loading of expensive platinum (Pt) catalyst (a crucial component required to achieve high power densities) has hindered extensive market applications [4,5]. Specifically, high cathode Pt loading (typically 0.4–0.5 mg_{Pt} cm^{-2}) are required to overcome the inherent sluggish oxygen reduction reaction kinetics (ORR) ($½O_2 + 2H^+ + 2e^- \rightarrow H_2O$) [6]. Therefore, reducing the Pt loading without sacrificing fuel cell performance (*i.e.*, Pt utilization enhancement) has attracted considerable interest over the last two decades.

Pt utilization can be enhanced through the optimization of Pt-ionomer-pore percolating networks within the fuel cell electrode, *i.e.*, triple phase boundaries (TPBs), where all indispensable reaction species (electron, proton, and oxygen) exist and ORR occurs [7–10]. To optimize TPBs, especially under ultra-low Pt loading conditions, a balance between void and solid volume in the electrode requires careful design. The void volume (pores) allows oxygen and water transport, while the solid volume (Pt-ionomer) provides proton and electron conduction. Conventional ink-based electrode fabrication usually results in an evaporation-formed random porous network. The internal structure of the porous network typically can be adjusted by catalyst ink preparation (*e.g.*, Nafion to Pt/C ratio [11–13], hydrophobic additives [14–16], ink dispersing media [17–19], and dispersion technique [20,21]), but provides minimum subject control over the electrode architecture design.

In addition to conventional design and optimization of catalyst ink, increasing attention has focused on artificially designed electrode interface or internal structures [22,23]. As an emerging approach for advanced electrode design, tailoring microstructure through patterning can rearrange the proton-electron-porosity percolating networks, and enable enhanced fuel cell performance [22,24]. Constructing patterned electrodes with periodic structures to optimize TPBs has been investigated with both two-dimensional (2D) and three-dimensional (3D) patterns. 2D geometrically patterned electrodes are usually catalyst ink-based and fabricated by inkjet printing [25–28] or by spraying the ink through flat micro-stencil masks [29–31]. In contrast, 3D patterned electrodes consist of larger z-direction depth, which could provide more void space and interconnected macropores, resulting in enhanced TPB connections compared to their 2D counterparts. Common approaches to extend 2D to 3D patterned electrodes include imprinting commercial Nafion membranes with patterned molds [32–34] or lithography etching [35], employing liquid precursors to build patterned membranes by micromolding techniques [33,36–39], and casting catalyst ink slurries into elastomeric molds [40]. Although feasible, patterned interfaces prepared by these methods are less durable due to the collapse of the Nafion surface in the subsequent hot-pressing bonding procedure for membrane electrode assemblies (MEAs) at the glass transition temperature of Nafion (T_g) (*ca.* 135 °C). More durable intricate alternative 3D patterning methods usually require a sacrificial template, which either Pt or Nafion ionomer will be deposited on to form a 3D framework. After removing the initial sacrificial template, the other species will be deposited on the outer surface of the framework from the previous step. For instance, an inverse oval patterned Pt electrode was constructed through self-assembled polystyrene beads, showing enhanced mass transfer and performance owing to the morphological advantages [41]. Patterned Nafion arrays constructed *via* anodic aluminum oxide (AAO) templates also demonstrated power density and lifetime improvements [42]. Even though these methods hold promise in improving power performance, the cathode Pt loading remains relatively high (0.2–0.4 mg_{Pt} cm^{-2}); higher than the 2020 DOE total Pt loading target (0.125 mg_{Pt} cm^{-2}) [43].

Can the advantages of 3D patterned structure be applied to ultra-low Pt loading electrodes? In our previous study, a simultaneous electrospinning/electrospraying (E/E) technique was developed to produce unique nanofiber-nanoparticle electrodes for ultra-low Pt loading (*ca.* < 0.1 mg_{Pt} cm^{-2}) fuel cells [44]. Unlike conventional ink-based electrodes, the interaction of nanofibers and nanoparticles increases the number and connectivity of TPBs inside the electrodes, which generated high power outputs even at ultra-low cathode Pt loading (0.022 mg_{Pt} cm^{-2}). However, previously developed E/E electrodes were randomly assembled due to the nature of whipping electrospinning jets. Therefore, it would be of great interest to develop E/E electrodes containing patterned fiber mats to improve water management and further enhance fuel cell performance at ultra-low Pt loadings. Although patterned fiber mats have been utilized for tissue engineering [45], to the best of our knowledge, it has not yet been investigated for patterned nanofiber-nanoparticle electrodes in fuel cells.

In this work, we demonstrate a novel template-assisted E/E technique as a strategy for creating organized patterned nanofiber-nanoparticle electrodes at ultra-low Pt loadings. More specifically, photolithographed patterned templates were utilized to direct the deposition of electrospun nanofibers and electrosprayed nanoparticles during the E/E process to generate 3D patterned electrodes. Four different hexagonally patterned electrode sizes were fabricated in this study (pattern diameters of 40, 80, 160, and 360 μm). The influence of patterned E/E electrode, as well as the pattern size on fuel cell performance were investigated. The patterned electrodes were fabricated into MEAs as cathodes and the subsequent performances were evaluated in a fuel cell. The electrochemical surface area, cell resistance and power densities of the patterned electrodes were also compared with the random electrodes prepared by E/E.

Experimental

Materials

Isopropanol (IPA; ACS reagent, ≥ 99.5%) and poly (ethylene oxide) (PEO; M_V = 400,000 g mol^{-1}) were purchased from Sigma-Aldrich. Carbon supported 20 wt% Pt catalyst (Pt/C; Vulcan XC-72) was purchased from Premetek. Nafion solution (LQ-1105) and Nafion membrane (NR-212) were purchased

from IonPower. Photoresist SU-8 3050 and SU-8 developer were purchased from MicroChem. Silicon wafer (n-type, 5″) was purchased from UniversityWafer. Gas diffusion layer (GDL; Sigracet 25BC) was purchased from Fuel Cells Etc. All materials were used as received. Deionized (DI) water with a resistivity of 16 MΩ cm was used as appropriate. Ultra-high purity grade nitrogen was purchased from Brazos Valley Welding Supply. Ultra-high purity oxygen and ultra-zero grade air were purchased from Airgas. Ultra-high purity hydrogen was purchased from Praxair. All gases were used for fuel cell experiments.

Fabrication of the pattern templates

The SU-8 3050 photoresists were applied on silicon wafers by spin coating (BID-TEK SP-100 Spin Coater) followed by a soft-baking procedure to achieve a 60 μm thick coating. Hexagonal micro-patterns were fabricated *via* photolithographic (EVG 610 Double-sided Mask Aligner) using customized photomasks (quartz-chrome substrate, PortalPhotomask) and then washed by SU-8 developers. The depth of the pattern was controlled by spin-coating speed and UV-exposing time. After photolithography, double conductive layers (Al-120 nm and Au-30 nm) were deposited on top using an electron beam evaporator (Lesker PVD 75 E-Beam Evaporator). The patterned surface was divided into four 2 cm by 2 cm square zones. Each zone was patterned with one characteristic hexagonal internal diameter 40 μm, 80 μm, 160 μm, and 360 μm, respectively. The width and height of the hexagonal pores were 20 μm and 60 μm, respectively.

Template-assisted electrospinning/electrospraying (E/E)

A custom-designed E/E apparatus, as illustrated in Fig. 1 (a), has been described in detail in previous work [46]. Patterned templates were fixed on the drum collector, where Nafion nanofibers and Pt/C nanoparticles were electrospun and electrosprayed simultaneously. The anode was fabricated by solely electrospraying, whereas the cathode was fabricated by template-assisted E/E. The anode electrospraying catalyst ink solution used to fabricate E/E electrodes consisted of a mixture of 20 mg of Pt/C catalyst, 400 mg of 5 wt% Nafion solution, 580 mg of isopropanol/DI water (3/1 v/v), with solids weight percent constant at 4 wt% for all E/E experiments. The mixture was sonicated for at least 3 min before electrospraying. For cathode, the catalyst ink composition was similar to the anode catalyst ink solution with the exclusion of the Nafion solution. The electrospinning polymer solution used to fabricate cathode electrodes was a 10 wt% 20/1 Nafion/PEO polymer solution, *e.g.*, 5 mg of PEO, 100 mg of dried Nafion flakes, and 945 mg of 3/1 v/v isopropanol/water. The polymer solution was stirred at ambient temperature for at least 12 h to ensure the complete dissolution of Nafion and PEO. The catalyst ink and the polymer solution were used in the electrospraying and electrospinning processes respectively, with the Pt loading controlled by the E/E duration. The needle tip to collector distances, applied voltages, and solution flow rates were 15 and 9 cm, 7 and 15 kV, 0.3 and 0.8 mL h^{-1} for the electrospinning and electrospraying processes, respectively.

Patterned electrode transfer and membrane electrode assembly (MEA) fabrication

After electrodes were fabricated *via* template-assisted E/E, the electrodes were transferred from the patterned templates to Nafion membranes. This was accomplished by gently pressing a bare Nafion membrane onto a patterned electrode and then gently peeling away the Nafion membrane together with the transferred patterned electrode, as shown in Fig. 1 (b). Nafion membranes with transferred patterned electrodes were then

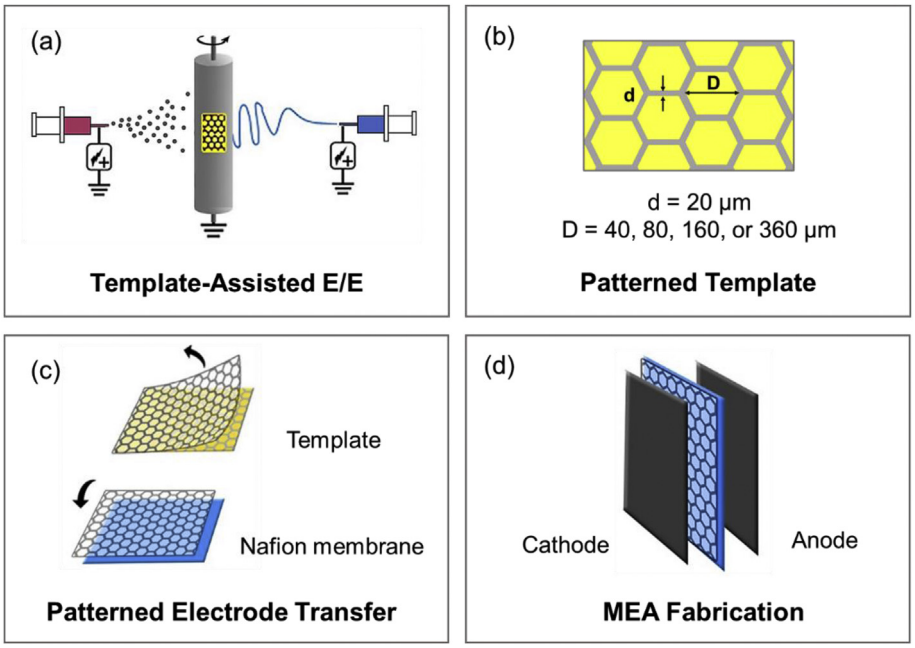

Fig. 1 – Experimental schematic: (a) template-Assisted E/E apparatus, (b) patterned template diameter sizes, (c) patterned electrode transfer from patterned template to Nafion membrane, and (d) MEA fabrication.

combined with GDLs to fabricate membrane electrode assemblies (MEAs) by sandwiching the Nafion membrane/patterned cathode between a bare GDL (cathode substrate) and an electrosprayed GDL (anode), and hot pressed (3851–0, Carver) for 5 min at 275 °F (135 °C) and 600–800 psi (4.1–5.5 MPa), as shown in Fig. 1 (c). At least three MEAs at each of five different cathode pattern sizes (D = random, 40, 80, 160, 360 μm) were fabricated for a total of fifteen E/E MEAs in this study.

Electrode characterization

The morphology of the patterned electrodes was characterized by an optical microscope (Eclipse Ti-E Inverted Microscope, Nikon Instruments) and scanning electron microscopy (SEM; FEI Quanta 600 FE-SEM). For cross-sectional area characterization, Nafion supported electrodes were soaked in liquid nitrogen for 15 min, and then cut with a doctoral blade immediately. All samples were sputter-coated (Cressington 208 HR) with 6 nm Platinum/Iridium before SEM analysis. To analyze the nanofiber and nanoparticle size distributions, 50 counts for each sample were randomly sampled and analyzed using ImageJ software.

The Pt loading was measured with thermal gravimetric analysis (TGA; Q50, TA Instrument). A small portion of the electrode (*ca.* 4–6 mg) was heated from 25 °C to 900 °C at 10 °C min^{-1} in the air at 60 mL min^{-1}. The Pt loading was determined by dividing the residual weight at 850 °C by the original sample area (all other components degrade below 800 °C except for Pt). The average Pt loading for each patterned electrode was determined using at least 2–4 electrodes.

Fuel cell tests and cyclic voltammetry (CV)

Each MEA (1.21 cm^2 area) was placed between two serpentine flow field graphite plates (1 cm^2 flow area) separated by two 0.152 mm thick PTFE/fiberglass gaskets (Cat. No. 33, Scribner Associates, Inc.). The entire fuel cell assembly consisted of an MEA, two gaskets, and two flow plates placed between copper current collectors followed by endplates all held together by bolts with 100 lb in (11.3 N m) of applied torque. Fuel cell performance of each MEA was evaluated with a fuel cell test station (850C, Scribner Associates, Inc.). Fuel cell tests were conducted under ambient pressure with saturated (100% RH) anode and cathode flow rates of 0.43 L min^{-1} hydrogen and 1.02 L min^{-1} oxygen at 80 °C, respectively. Fuel cell performance was recorded after a new MEA was fully activated. The activation process consists of operating the MEA at 0.7 V for 1 h, followed by 0.6 V, 0.4 V, and 0.2 V for 30 min at each voltage, and ending with two cycles of 0.6 V and 0.4 V for 30 min at each voltage. Polarization curves (cell voltage versus current density) were collected from the open-circuit voltage (OCV) to 0.2 V at increments of 0.05 V min^{-1} to determine that no further increase in current density at a constant voltage was observed, thus the MEA was at steady state. After the MEA was fully activated and reached a steady state, five polarization curves were collected to determine the average maximum power density. The average error between polarization curves was <3% for the hydrogen/oxygen experiments.

Cyclic voltammetry (CV) was performed on a fully activated MEA with a potentiostat (Solartron SI 1287A, Corrware Software) at 20 mV s^{-1} from 0.01 V to 1 V versus NHE under ambient pressure. In this two-electrode configuration, the anode serves as both the counter and reference electrodes. The fuel cell anode and cathode were supplied with 0.04 L min^{-1} hydrogen and 0.02 L min^{-1} nitrogen, respectively. Temperatures of the cathode gas, anode gas, and cell were maintained at 30 °C. The Pt catalyst was assumed to have an average site density of 210 μC cm^{-2} [47]. The electrochemical surface area (ECSA) was determined from the hydrogen adsorption area from 0.1 to 0.3 V. Five cycles were taken to determine the average ECSA for each MEA. Linear sweep voltammetry was performed at 2 mV s^{-1} from OCV to 0.8 V versus NHE to determine if the MEA had any defects that resulted from internal shorts or significant hydrogen crossover.

Electrochemical impedance spectroscopy

Electrochemical impedance spectroscopy (EIS; Solartron SI 1260A) was performed on a fully activated MEA from 1 MHz to 1 Hz at 0.4 V *versus* NHE under ambient pressure. In this two-electrode configuration, the anode serves as both the counter and reference electrodes. The fuel cell anode and cathode were supplied with 0.43 L min^{-1} hydrogen and 1.02 L min^{-1} oxygen, respectively. Temperatures of the cathode gas, anode gas, and cell were all maintained at 80 °C. The EIS data was analyzed using the classic equivalent circuit models that consisted of a resistor (resistance of the solid electrolyte membrane) in series with a parallel circuit of a constant phase element and a second resistor (resistance of the electrode) that is typically used to describe a porous electrode [48].

Results and discussion

Patterned electrode morphology

Fig. 2 shows images of the patterned electrode morphologies fabricated *via* template-assisted E/E. Fig. 2(a) shows the patterned electrodes supported on a transparent Nafion membrane substrate fabricated by decal transfer (Fig. 1(c)). The decal transfer was facile due to the higher affinity of the electrode to the flexible Nafion membrane compared to the rigid metal-coated silicon wafer templates. Brightfield optical microscopy images of all electrodes are shown in Fig. 2(b–f), where each image corresponds to a specific feature size (hexagonal pattern diameter D = 40 μm, 80 μm, 160 μm, 360 μm; random). In contrast to the morphology of the random oriented electrode (shown in Fig. 2(f)), the organized hexagonal patterned features are clearly demonstrated in Fig. 2(b–e). Nafion nanofibers and Pt/C nanoparticles collect on patterned template and form honeycomb structured electrode (darker area in Fig. 2(b–e)) demonstrating the template-assisted E/E technique and its ability to guide the well-controlled nanofiber-nanoparticle deposition in the range of few tens to few hundreds of microns.

Fig. 3 shows the SEM images of the top and cross-sectional views of the E/E patterned electrodes. Individual hexagonal patterned structures with different feature sizes under high

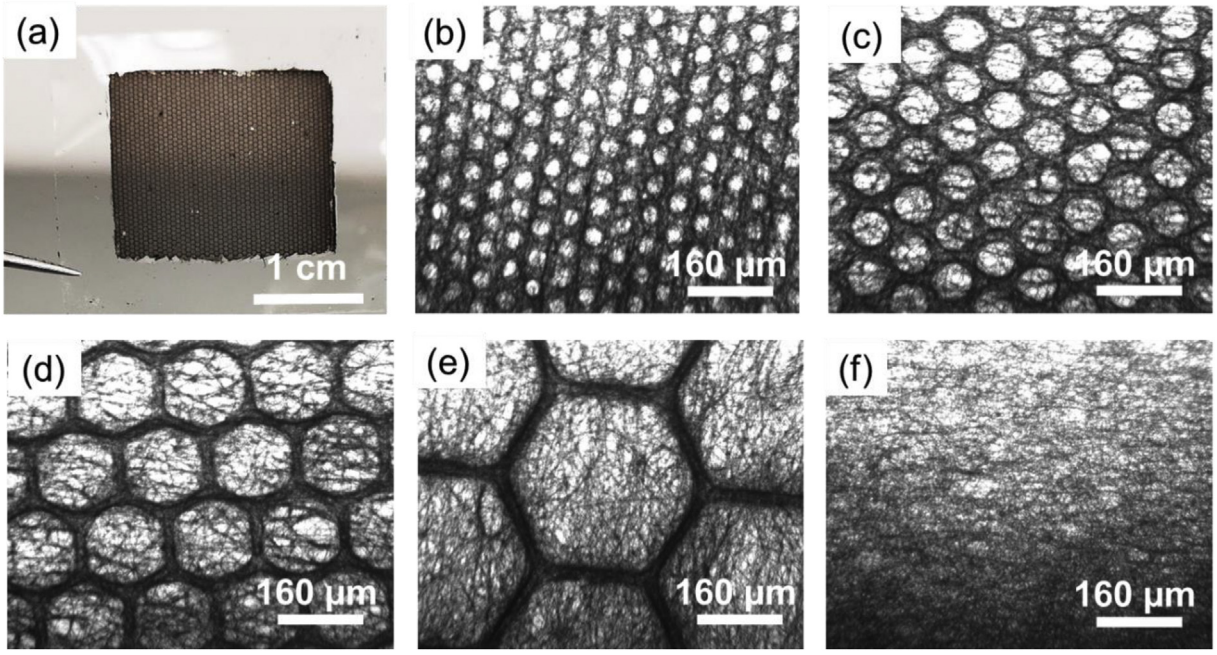

Fig. 2 – Images of patterned electrode morphology. (a) Photo of the patterned electrode transferred onto Nafion membrane substrate, and optical microscope images for E/E electrodes with hexagonal pattern diameters of (b) 40 μm, (c) 80 μm, (d) 160 μm, (e) 360 μm and (f) random morphology.

magnification were shown in Fig. 3(a–d). The E/E catalyst layers show a highly porous microscopic morphology with interconnected nanofibers and particle aggregates. More importantly, the hexagonal patterns organize nanofibers and nanoparticles into catalyst-dense walls and catalyst-thin openings, which could act as reservoirs for the collection and removal of produced water during fuel cell operation, specifically at high current density where the water generation rate is more significant. The solid phase electron and proton conduction could be enhanced through the organized nanofiber/nanoparticle bundles, whereas the gas phase mass transport resistance could be mitigated through the catalyst-thin openings, where both effects in combination could promote enhanced TPBs. Moreover, by incorporating rigid catalyst particles into 3D scaffolds, the mechanical strength of the patterned electrodes could be enhanced, which may facilitate the preservation of the organized structure during subsequent processing and fuel cell operation.

Fig. 3(e–h) demonstrate electrodes with the visible replicated pattern under lower magnification, which confirms that the collector efficiently directs the internal microconstruction of the nanofiber-nanoparticle electrodes. As the pattern diameter increases, the conductive area guiding the nanofiber deposition decreases, which results in less control of forming a well-defined hexagonal patterned fiber mat. Fig. 3(i–l) displays the freeze-fractured cross-sectional area of the electrodes, representing the depth-direction structure consisting of nanofibers and nanoparticles with a similar average thickness ranging between 10 to 20 μm regardless of the pattern size.

Fig. 4(a and b) shows the average Nafion nanofiber and Pt/C catalyst nanoparticle diameters based on quantitative analysis of the SEM images shown in Fig. 3(a–d). The results show that the average fiber diameters range from 220 ± 35 nm to 272 ± 38 nm and the average particle diameters range from 0.81 ± 0.20 μm to 0.98 ± 0.21 μm, indicating that the fiber and catalyst aggregate sizes are similar for all electrodes regardless of the hexagonal feature sizes. These results suggest that the template-assisted E/E technique can solely adjust micron-scale pattern structure without affecting the nano-scale morphology, validating the sole investigation of the pattern size effect.

Fuel cell performance and electrochemical characterization

Fig. 5 shows the polarization and power density curves of MEAs with patterned electrodes measured under standard operating conditions (*i.e.*, fully humidified H_2/O_2 at 80 °C under ambient pressure), with cathode Pt loadings of *ca.* 0.06 mg_{Pt} cm^{-2} (see Table 1 for detailed results). Patterned E/E electrodes with four pattern diameters achieved peak power densities ranging from 418 mW cm^{-2} (360 μm) to 481 mW cm^{-2} (80 μm). Specifically, the electrode with an 80 μm diameter pattern outperformed the rest of other pattern sizes, exhibiting a maximum power density of 481 mW cm^{-2} and an 18% improvement compared to the random electrode with a power density of 402 mW cm^{-2}. This maximum peak power density is comparable with studies by González et al. [13], Hwang et al. [46], and Cooper et al. [49] with ultra-low Pt loading. For electrode with larger pattern sizes (*i.e.*, 160 μm and 360 μm), less of an enhancement over the random electrode was observed likely due to the sparse hexagonal openings (Fig. 3(c and d)), which may impact mass transport and the TPBs in the electrode.

To further understand the impact of the patterned morphology on fuel cell performance, *in situ* cyclic

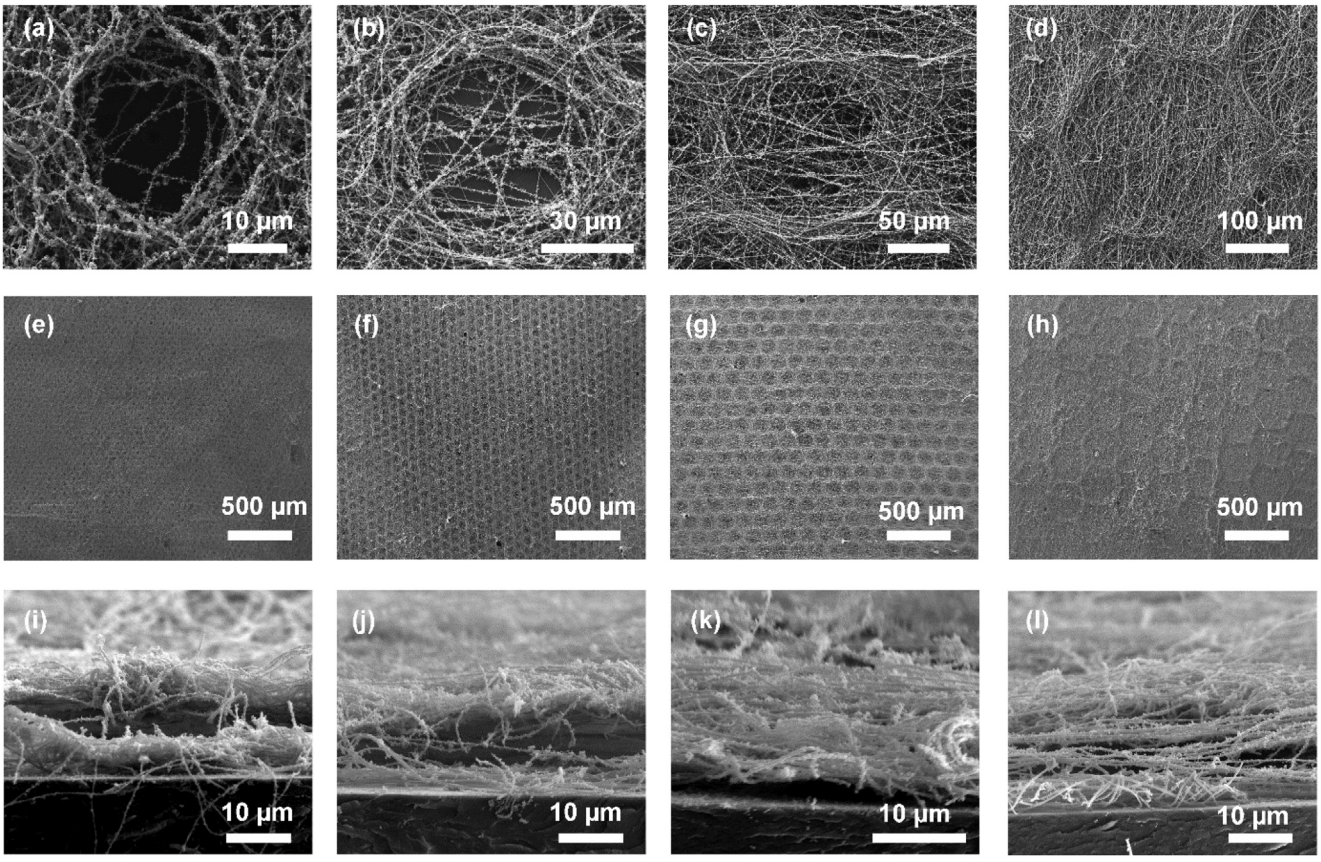

Fig. 3 – SEM images of E/E patterned electrodes with diameters of 40 μm (a,e,i), 80 μm (b,f,j), 160 μm (c,g,k), and 360 μm (d,h,l): (a–d) top view of individual hexagonal feature, (e–h) top view of patterned electrode surface and (i–j) cross-sectional view of patterned electrodes.

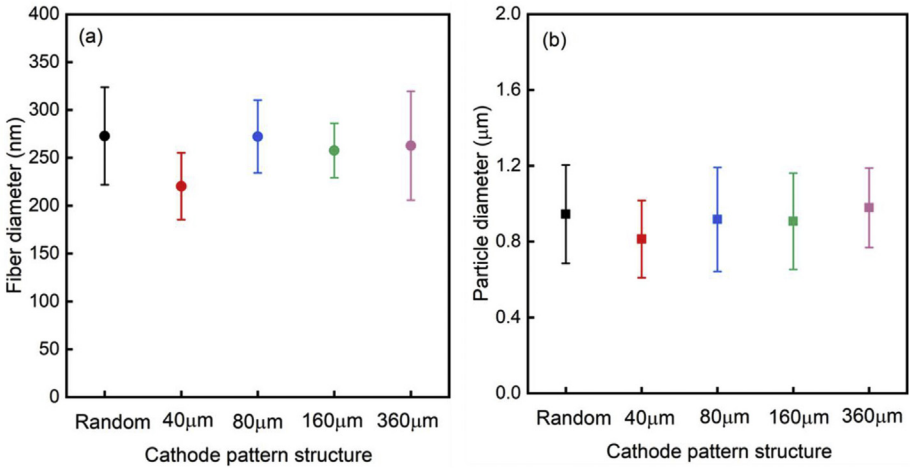

Fig. 4 – (a) Nafion nanofiber diameters and (b) Pt/C catalyst nanoparticle diameters in electrodes as a function of cathode pattern structure.

voltammetry (CV) was performed to characterize the electrochemical surface area (ECSA). Fig. 6 shows CVs of MEAs with the random electrode and patterned electrodes at various pattern diameters, 40 μm, 80 μm, 160 μm, and 360 μm. The cathode Pt loading were maintained at a similar level (*ca.* 0.06 mg_{Pt} cm^{-2}) for consistent comparison. During CV measurements, the adsorption and desorption of hydrogen ($H_2 \leftrightarrow 2H^+ + 2e^-$) occur at available Pt sites in the range from 0.1 to 0.3 V. As demonstrated in Table 1, the ECSAs of the 40 μm pattern size (22.6 m^2 g_{Pt}^{-1}) and 80 μm pattern size (33.7 m^2 g_{Pt}^{-1})

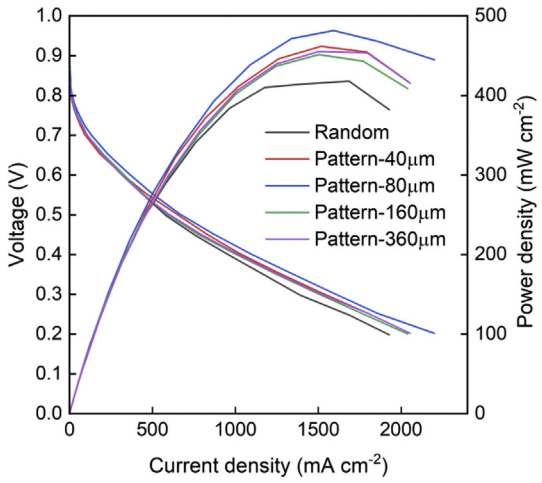

Fig. 5 – Fuel cell polarization and power density curves for MEAs with the random electrode (black) and patterned electrodes at 40 μm (red), 80 μm (blue), 160 μm (green), 360 μm (purple) pattern diameter, measured with 100% RH hydrogen/oxygen at 80 °C under ambient pressure. (For interpretation of the references to colour in this figure legend, the reader is referred to the Web version of this article.)

electrodes increase compared to the random electrode (20.0 m^2 g_{Pt}^{-1}). At 80 μm pattern size, the ECSA reached the highest value and exhibits a 68% increase compared to the random electrode. This increase can be attributed to the increase in electrode macroporosity, which may allow for more liquid water product during fuel cell operation to be expelled out and alleviate the flooding issue at high current densities; also, more oxygen could penetrate though the electrode and improve access to active Pt catalyst sites. With the further increase of pattern size to 160 μm and 360 μm, the ECSAs decreases from 33.7 m^2 g_{Pt}^{-1} (80 μm) to 29.8 m^2 g_{Pt}^{-1} (160 μm) and 22.8 m^2 g_{Pt}^{-1} (360 μm), respectively, which are still 49% and 14% higher than the random control. Overall, the ECSAs provide direct evidence for higher Pt utilization in patterned electrodes compared to random electrodes under similar cathode Pt loading, and corroborate with the fuel cell power performance results (Fig. 5).

Fig. 7 (a) shows the averaged maximum power densities as a function of the cathode electrode pattern structure. As the pattern size evolves from random to 40 μm pattern, the averaged peak power densities increased from 405 mW cm^{-2} to 451 mW cm^{-2}, then reached the maximum at 462.6 mW cm^{-2} for 80 μm pattern. Further increasing pattern sizes to 160 μm pattern induced a slight power density drop to 439 mW cm^{-2}, and further down to 418.4 mW cm^{-2} for the largest 360 μm pattern. However, one could argue that these power densities differences are not significant in light of the statistical error among repeated experiments shown in the graph. Therefore, a better measure is to normalize the peak power densities, *i.e.*, Pt utilization or normalized peak power densities as shown in Fig. 7 (b). Following a similar trend as Fig. 5, significant increases in the normalized maximum power density was observed for electrodes with smaller pattern sizes. The normalized maximum power density was 6.78 ± 0.69 kW g_{Pt}^{-1} for electrodes with 40 μm pattern, and then

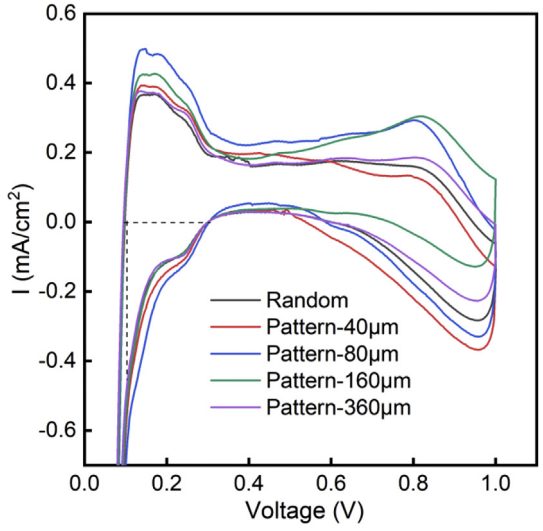

Fig. 6 – Cyclic voltammograms for MEAs with the random electrode (black) and patterned electrodes at 40 μm (red), 80 μm (blue), 160 μm (green), 360 μm (purple) pattern diameters. The ECSA integration area (0.1–0.3 V) for hydrogen adsorption peak is indicated by the dashed black lines. (For interpretation of the references to colour in this figure legend, the reader is referred to the Web version of this article.)

Table 1 – Fuel cell and electrochemical performances of E/E patterned electrodes.

Cathode structure	Pt loading (mg_{Pt} cm^{-2})		Max power density[a] (mW cm^{-2})	Pt utilization[a,c] (kW g_{Pt}^{-1})	ECSA[b] (m^2 g_{Pt}^{-1})	Electrode resistance[a] (mΩ cm^{-2})
	Anode	Cathode				
Random	0.034	0.060	405.1 ± 11.0	5.82 ± 0.16	20.0	320.8
Pattern-40 μm	0.027	0.061	451.0 ± 45.9	6.78 ± 0.69	22.6	368.9
Pattern-80 μm	0.024	0.056	462.6 ± 69.4	8.26 ± 1.24	33.7	322.4
Pattern-160 μm	0.043	0.028	439.1 ± 51.5	5.87 ± 0.69	29.8	353.8
Pattern-360 μm	0.026	0.061	418.4 ± 72.6	7.23 ± 1.25	22.8	445.7

[a] Under H_2/O_2 at 80 °C, ambient pressure.
[b] Under H_2/N_2 at 30 °C, ambient pressure.
[c] Normalized by the total Pt loading inside MEA.

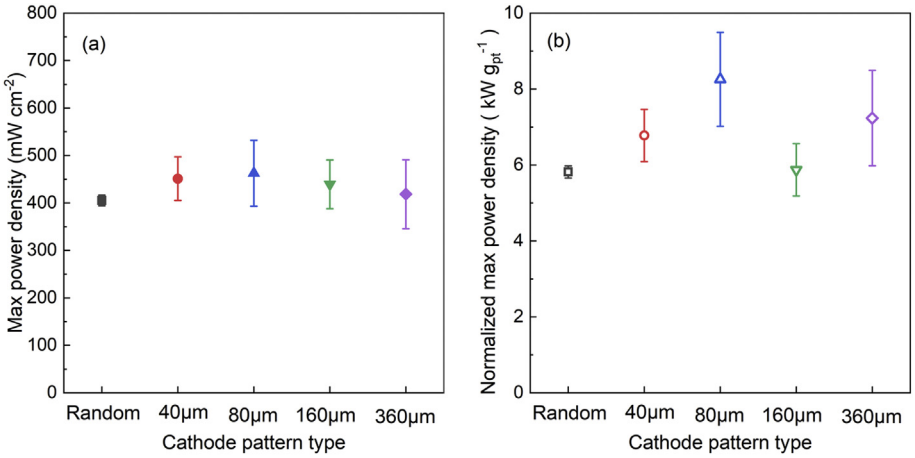

Fig. 7 – (a) Maximum power density (solid symbols) and (b) Pt utilization (hollow symbols) for random (black square) and patterned electrodes with 40 μm (red circle), 80 μm (blue triangle), 160 μm (green inverted triangle), and 360 μm (purple diamond) diameter sizes. (For interpretation of the references to colour in this figure legend, the reader is referred to the Web version of this article.)

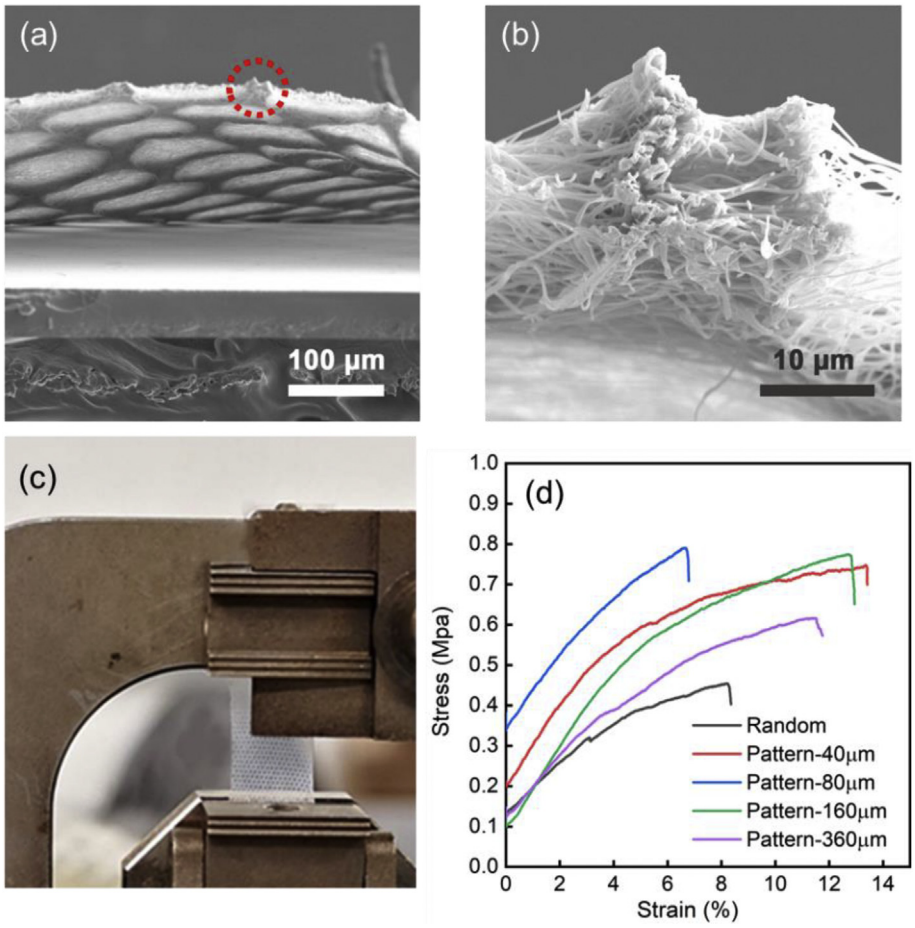

Fig. 8 – (a) SEM image of a perspective view of freeze-fractured patterned fiber networks looking underneath, (b) higher magnification of the circled area in (a) showing the fiber mat thickness, (c) electrospun patterned high purity Nafion fiber networks (95 wt% Nafion) fixed to the dynamic mechanical analyzer (DMA) and (d) stress-strain profiles of Nafion fiber networks with the random (black) and patterned morphology at 40 μm (red), 80 μm (blue), 160 μm (green) and 360 μm (purple) pattern diameter sizes, measured at 25 °C, 47% RH. (For interpretation of the references to colour in this figure legend, the reader is referred to the Web version of this article.)

reached a peak value at 8.26 ± 1.24 kW g_{Pt}^{-1} for 80 μm pattern, showing 42% increment compared to the random cathode structure (5.82 ± 0.16 kW g_{Pt}^{-1}). This difference is statistically significant. For the larger pattern sizes of 160 and 360 μm, Pt utilization of 5.87 ± 0.69 and 7.23 ± 1.25 kW g_{Pt}^{-1} was observed, respectively. Overall, the Pt utilization advantages of the patterned electrodes compared to the random electrodes are clearly demonstrated.

The electrode resistance was measured by the electrochemical impedance spectroscopy (EIS) (Table 1). The measurements were conducted under hydrogen/oxygen at ambient pressure at 80 °C at 0.4 V *versus* NHE, a voltage at which the ohmic and transport resistances are dominant. The random electrode showed a resistance of 320.8 mΩ cm^{-2}, similar to the results in a previous study (321.48 mΩ cm^{-2} with 0 wt% Nafion in the electrospraying catalyst ink) [46]. The 80 μm patterned electrode demonstrated the lowest resistance of 322.4 mΩ cm^{-2}, suggesting more triple phase boundary connections with lower proton and mass transfer resistance throughout the hexagonal pattern. The 360 μm patterned electrode showed the highest resistance of 445.7 mΩ cm^{-2} among all patterned electrodes; the larger pattern size may result in less triple phase boundary connections comparatively and lower connectivity of the proton conducting nanofibrous network. The fuel cell performance (averaged anode and cathode Pt loading, maximum power density, Pt utilization, ECSA, and electrode resistance) of the patterned electrodes and random electrode are listed in Table 1.

Mechanical properties of patterned nanofibers

Mechanical properties can reflect the processability of patterned electrodes and the ability to maintain a robust and integrated configuration during fuel cell operation. The cross-sectional SEM images of the patterned Nafion fiber mats are shown in Fig. 8(a and b), with a thickness of *ca.* 15 μm. To get more insight into the effect of patterns on the mechanical properties of the fibrous structure, tensile strength measurements were performed on the patterned high purity Nafion (95%) nanofiber constructs produced *via* template-assisted electrospinning (as shown in Fig. 8). Young's modulus, ultimate tensile strength and elongation to break properties of the fiber network are listed in Table 2. The 40 μm, 80 μm and 160 μm patterned fiber network showed Young's modulus of 9.27 MPa, 9.27 MPa, and 9.06 MPa, respectively, revealing higher stiffness compared to the random control (5.43 MPa) and 360 μm patterned fiber network (5.71 MPa). All patterned fiber network showed similar elongation to break compared to the random control without significant difference. Intuitively, we expected the fiber network mechanical properties to be compromised due to the patterned structure, however, the patterned porous structures appear to have improved stiffness and ultimate tensile strength compared to the random network structure. This result could be attributed to the increased strength through the fiber bundles due to the patterned structure. The patterned fiber network with organized fiber bundles improved the alignment of the fibers in the tensile direction, whereas the random constructs failed to control individual fiber orientation.

Table 2 – Mechanical properties of high purity Nafion fiber networks.

Cathode structure	Young's modulus (MPa)	Ultimate tensile strength (MPa)	Elongation to break (%)
Random	5.43	0.455	8.7
Pattern-40 μm	9.27	0.747	13.4
Pattern-80 μm	9.27	0.790	6.7
Pattern-160 μm	9.06	0.774	12.9
Pattern-360 μm	5.71	0.616	11.5

Conclusions

In this study, we demonstrated a template-assisted E/E technique for fabricating unique nanofiber-nanoparticle PEMFC electrodes with 3D hexagonal patterned features, ranging from 40 μm to 360 μm in diameter. Owing to the open and interconnected hexagonal architecture, the nanofiber-nanoparticle patterned electrodes show enhancements compared to non-patterned electrodes possibly due to enhanced triple phase boundaries and enhanced porosity and water management. With an ultra-low cathode Pt loading of 0.06 mg_{Pt} cm^{-2}, hexagonal patterned electrodes with 80 μm diameter demonstrated a Pt utilization of 8.26 kW g_{Pt}^{-1}, showing 42% increase when compared to the randomly assembled electrode (5.82 kW g_{Pt}^{-1}). Furthermore, the mechanical strength of the Nafion fiber mats were not compromised by the pattern structure. Patterned electrode fabricated by template-assisted E/E technique show great promise for the future development of low-cost fuel cell vehicles with high power density and ultra-low Pt loading.

Declaration of competing interest

The authors declare that they have no known competing financial interests or personal relationships that could have appeared to influence the work reported in this paper.

Acknowledgements

This work was supported in part by National Science Foundation under award no. CMMI-1661822.

REFERENCES

[1] Mehta V, Cooper JS. Review and analysis of PEM fuel cell design and manufacturing. J Power Sources 2003;114:32–53.
[2] Cipriani G, Di Dio V, Genduso F, La Cascia D, Liga R, Miceli R, et al. Perspective on hydrogen energy carrier and its automotive applications. Int J Hydrogen Energy 2014;39:8482–94.

[3] Hwang M, Nixon K, Sun R, Willis C, Elabd YA. Sulfonated pentablock terpolymers as membranes and ionomers in hydrogen fuel cells. J Membr Sci 2021;633:119330.
[4] Debe MK. Electrocatalyst approaches and challenges for automotive fuel cells. Nature 2012;486:43–51.
[5] Wang Y, Chen KS, Mishler J, Cho SC, Adroher XC. A review of polymer electrolyte membrane fuel cells: technology, applications, and needs on fundamental research. Appl Energy 2011;88:981–1007.
[6] Gottesfeld S, Zawodzinski TA. Polymer electrolyte fuel cells. Adv Electrochem Sci Eng 1997;5:195–302.
[7] Wilson MS, Gottesfeld S. Thin-film catalyst layers for polymer electrolyte fuel cell electrodes. J Appl Electrochem 1992;22:1–7.
[8] Dhanda A, Pitsch H, O'Hayre R. Diffusion impedance element model for the triple phase boundary. J Electrochem Soc 2011;158.
[9] Blom DA, Dunlap JR, Nolan TA, Allard LF. Preparation of cross-sectional samples of proton exchange membrane fuel cells by ultramicrotomy for TEM. J Electrochem Soc 2003;150.
[10] Majlan EH, Rohendi D, Daud WRW, Husaini T, Haque MA. Electrode for proton exchange membrane fuel cells: a review. Renew Sustain Energy Rev 2018;89:117–34.
[11] Antolini E, Giorgi L, Pozio A, Passalacqua E. Influence of Nafion loading in the catalyst layer of gas-diffusion electrodes for PEFC. J Power Sources 1999;77:136–42.
[12] Xie J, Xu F, Wood III DL, More KL, Zawodzinski TA, Smith WH. Influence of ionomer content on the structure and performance of PEFC membrane electrode assemblies. Electrochim Acta 2010;55:7404–12.
[13] González Rodríguez L, Campana Prada R, Sanchez-Molina M, Rodríguez Victoria TA. Study of the influence of Nafion/C composition on electrochemical performance of PEM single cells with ultra-low platinum load. Int J Hydrogen Energy 2021;46:17550–61.
[14] Therdthianwong A, Saenwiset P, Therdthianwong S. Cathode catalyst layer design for proton exchange membrane fuel cells. Fuel 2012;91:192–9.
[15] Öztürk A, Fıçıcılar B, Eroğlu İ, Bayrakçeken Yurtcan A. Facilitation of water management in low Pt loaded PEM fuel cell by creating hydrophobic microporous layer with PTFE, FEP and PDMS polymers: effect of polymer and carbon amounts. Int J Hydrogen Energy 2017;42:21226–49.
[16] Avcioglu GS, Ficicilar B, Eroglu I. Effect of PTFE nanoparticles in catalyst layer with high Pt loading on PEM fuel cell performance. Int J Hydrogen Energy 2016;41:10010–20.
[17] Ngo TT, Yu TL, Lin H-L. Influence of the composition of isopropyl alcohol/water mixture solvents in catalyst ink solutions on proton exchange membrane fuel cell performance. J Power Sources 2013;225:293–303.
[18] Sharma R, Andersen SM. Zoom in catalyst/ionomer interface in polymer electrolyte membrane fuel cell electrodes: impact of catalyst/ionomer dispersion media/solvent. ACS Appl Mater Interfaces 2018;10:38125–33.
[19] Jung C-Y, Kim W-J, Yi S-C. Optimization of catalyst ink composition for the preparation of a membrane electrode assembly in a proton exchange membrane fuel cell using the decal transfer. Int J Hydrogen Energy 2012;37:18446–54.
[20] Wang M, Park JH, Kabir S, Neyerlin KC, Kariuki NN, Lv H, et al. Impact of catalyst ink dispersing methodology on fuel cell performance using in-situ X-ray scattering. ACS Appl Energy Mater 2019;2:6417–27.
[21] Stähler M, Stähler A, Scheepers F, Carmo M, Stolten D. A completely slot die coated membrane electrode assembly. Int J Hydrogen Energy 2019;44:7053–8.
[22] Breitwieser M, Klingele M, Vierrath S, Zengerle R, Thiele S. Tailoring the membrane-electrode interface in PEM fuel cells: a review and perspective on novel engineering approaches. Adv Energy Mater 2018;8:1701257.
[23] Chen M, Zhao C, Sun F, Fan J, Li H, Wang H. Research progress of catalyst layer and interlayer interface structures in membrane electrode assembly (MEA) for proton exchange membrane fuel cell (PEMFC) system. eTransportation 2020;5:100075.
[24] Bae WG, Kim HN, Kim D, Park SH, Jeong HE, Suh KY. 25th anniversary article: scalable multiscale patterned structures inspired by nature: the role of hierarchy. Adv Mater 2014;26:675–700.
[25] Towne S, Viswanathan V, Holbery J, Rieke P. Fabrication of polymer electrolyte membrane fuel cell MEAs utilizing inkjet print technology. J Power Sources 2007;171:575–84.
[26] Taylor AD, Kim EY, Humes VP, Kizuka J, Thompson LT. Inkjet printing of carbon supported platinum 3-D catalyst layers for use in fuel cells. J Power Sources 2007;171:101–6.
[27] Shukla S, Domican K, Secanell M. Effect of electrode patterning on pem fuel cell performance using ink-jet printing method. ECS Transactions 2014;64:341–52.
[28] Bae I, Kim B, Kim D-Y, Kim H, Oh K-H. In-plane 2-D patterning of microporous layer by inkjet printing for water management of polymer electrolyte fuel cell. Renew Energy 2020;146:960–7.
[29] Kim J, Yamagata Y, Kim B, Higuchi T. Direct and dry micro-patterning of nano-particles by electrospray deposition through a micro-stencil mask. J Micromech Microeng 2009;19:025021.
[30] Yan W-C, Xie J, Wang C-H. Electrical field guided electrospray deposition for production of gradient particle patterns. ACS Appl Mater Interfaces 2018;10:18499–506.
[31] Shah K, Shin W, Besser R. Novel microfabrication approaches for directly patterning PEM fuel cell membranes. J Power Sources 2003;123:172–81.
[32] Bae JW, Cho Y-H, Sung Y-E, Shin K, Jho JY. Performance enhancement of polymer electrolyte membrane fuel cell by employing line-patterned Nafion membrane. J Ind Eng Chem 2012;18:876–9.
[33] Aizawa M, Gyoten H, Salah A, Liu X. Pillar structured membranes for suppressing cathodic concentration overvoltage in PEMFCs at elevated temperature/low relative humidity. J Electrochem Soc 2010;157:B1844.
[34] Koh JK, Jeon Y, Cho YI, Kim JH, Shul Y-G. A facile preparation method of surface patterned polymer electrolyte membranes for fuel cell applications. J Mater Chem 2014;2:8652–9.
[35] Omosebi A, Besser RS. Electron beam patterned Nafion membranes for DMFC applications. J Power Sources 2013;228:151–8.
[36] Zhou Z, Dominey RN, Rolland JP, Maynor BW, Pandya AA, DeSimone JM. Molded, high surface area polymer electrolyte membranes from cured liquid precursors. J Am Chem Soc 2006;128:12963–72.
[37] Rolland JP, Hagberg EC, Denison GM, Carter KR, De Simone JM. High-resolution soft lithography: enabling materials for nanotechnologies. Angew Chem Int Ed 2004;43:5796–9.
[38] Chen M, Wang M, Yang Z, Ding X, Li Q, Wang X. A novel catalyst layer structure based surface-patterned Nafion® membrane for high-performance direct methanol fuel cell. Electrochim Acta 2018;263:201–8.
[39] Yildirim MH, te Braake J, Aran HC, Stamatialis DF, Wessling M. Micro-patterned Nafion membranes for direct methanol fuel cell applications. J Membr Sci 2010;349:231–6.
[40] Paul MT, Kim D, Saha MS, Stumper J, Gates BD. Patterning catalyst layers with microscale features by soft lithography techniques for proton exchange membrane fuel cells. ACS Appl Energy Mater 2020;3(1):478–86.

[41] Kim O-H, Cho Y-H, Kang SH, Park H-Y, Kim M, Lim JW, et al. Ordered macroporous platinum electrode and enhanced mass transfer in fuel cells using inverse opal structure. Nat Commun 2013;4:1–9.
[42] Ning F, Bai C, Qin J, Song Y, Zhang T, Chen J, et al. Great improvement in the performance and lifetime of a fuel cell using a highly dense, well-ordered, and cone-shaped Nafion array. J Mater Chem 2020;8(11):5489–500.
[43] Energy UDo. DOE technical targets for polymer electrolyte membrane fuel cell components. 2019.
[44] Wang X, Richey FW, Wujcik KH, Elabd YA. Ultra-low platinum loadings in polymer electrolyte membrane fuel cell electrodes fabricated via simultaneous electrospinning/electrospraying method. J Power Sources 2014;264:42–8.
[45] Wittmer CR, Hébraud A, Nedjari S, Schlatter G. Well-organized 3D nanofibrous composite constructs using cooperative effects between electrospinning and electrospraying. Polymer 2014;55:5781–7.
[46] Hwang M, Elabd YA. Impact of ionomer resistance in nanofiber-nanoparticle electrodes for ultra-low platinum fuel cells. Int J Hydrogen Energy 2019;44:6245–56.
[47] Bett J, Kinoshita K, Routsis K, Stonehart P. A comparison of gas-phase and electrochemical measurements for chemisorbed carbon monoxide and hydrogen on platinum crystallites. J Catal 1973;29:160–8.
[48] Springer T, Zawodzinski T, Wilson M, Gottesfeld S. Characterization of polymer electrolyte fuel cells using AC impedance spectroscopy. J Electrochem Soc 1996;143:587.
[49] Cooper CD, Burk JJ, Taylor CP, Buratto SK. Ultra-low Pt loading catalyst layers prepared by pulse electrochemical deposition for PEM fuel cells. J Appl Electrochem 2017;47:699–709.